Combined frequency- and time-domain photocarrier radiometry characterization of ion-implanted and thermally annealed silicon wafers*

Ren Sheng-Dong(任胜东)[a)b)], Li Bin-Cheng(李斌成)[a)†], Gao Li-Feng(高丽峰)[a)], and Wang Qian (王 谦)[a)b)]

[a)] *Institute of Optics and Electronics, Chinese Academy of Sciences, Chengdu* 610209, *China*
[b)] *University of the Chinese Academy of Sciences, Beijing* 100049, *China*

(Received 5 November 2012; revised manuscript received 3 December 2012)

A combined frequency-swept and quasi-time-domain photocarrier radiometry (PCR) technique was developed to characterize thermally annealed silicon wafers with B^+, P^+, and As^+ ion implantation at doses ranging from 1×10^{11} cm^{-2} to 1×10^{16} cm^{-2}. The implantation dose dependence of the PCR amplitude, the frequency dependencies of the PCR amplitude and phase, as well as the quasi-time-domain PCR waveforms were simultaneously employed to analyze all the ion-implanted silicon samples. The dependence of the effective lifetime on the implantation dose has been investigated and shown to be related to the trap density and the lifetime extracted from the transient PCR signals.

Keywords: photocarrier radiometry, ion implantation, effective lifetime, silicon

PACS: 72.20.Jv, 78.55.Ap, 73.20.Hb, 73.50.Gr **DOI:** 10.1088/1674-1056/22/5/057202

1. Introduction

In the past, significant efforts have been devoted to the development of light emitters based on silicon (Si) wafers. Ng *et al*.[1] reported the efficient light emission in Si at room temperature via dislocation engineering, employing ion implantation, and subsequent thermal annealing. In recent years, a lot of studies[2–5] have been carried out to explore the dislocation loop dependence of the ion implantation process. Meanwhile, ion implantation became essential in microelectronic device fabrication to modify the electrical properties. The development of non-destructive and non-contact characterization techniques to better understand the evolution of the damage caused by ion implantation and thermal annealing and to monitor these processes is highly desirable.

Modulated photocarrier radiometry (PCR) technique has been used as a contactless diagnostic methodology for semiconductor characterization.[6–10] PCR relies on detection of the infrared emission from the semiconductor samples when they are optically excited by a modulated laser beam with photon energy larger than the fundamental energy gap of the material. The technique can determine the electrical and optical properties of semiconductor samples. In the past, PCR was applied mainly to characterize un-implanted semiconductor wafers or implanted but non-annealed wafers.[11] In this paper, a combined frequency-swept and quasi-time-domain PCR method was developed to investigate the structural evolution of silicon wafers with ion implantation and thermal annealing.

2. Experiment

In the experiment, three groups of ion-implanted and thermally annealed silicon wafers were used as samples. Groups S1 and S2 were prepared from ⟨100⟩ oriented n-type silicon wafers (525±20 μm, 8 Ω·cm–13 Ω·cm) with the front surface chemo-mechanically polished and thermally oxidized, and implanted with either phosphor (S1) or boron (S2) ions. Group S3 was prepared from ⟨111⟩ oriented p-type silicon wafers (525±20 μm, 8 Ω·cm–13 Ω·cm) with the front surface chemo-mechanically polished and implanted with arsenic ions. These samples were implanted with implantation doses from 1×10^{11} cm^{-2} to 1×10^{16} cm^{-2} and implantation energy of 100 keV. The ion-implanted samples were annealed in a rapid thermal annealing (RTA) system for 30 s in an inert nitrogen atmosphere. Groups S1 and S2 were annealed at 1000 °C and S3 was annealed at 1100 °C.

The experimental setup for PCR measurements was described in detail elsewhere.[6] In brief, a 104-mW-power and 830-nm-wavelength semiconductor laser with output power square-wave modulated by a function generator was used as the excitation source. The laser beam was focused with normal incidence onto the sample surface where the radius of the beam was measured to be approximately 22 μm. The infrared emissions at the excited site of the sample were focused through a pair of off-axis paraboloidal mirrors onto a photomultiplier (NIR PMT Module H10330A, Hamamatsu) with spectral response range from 950 nm to 1700 nm, and demodulated by a lock-in amplifier (LIA, Model 7280, Signal Recovery). The amplitude and phase of the LIA outputs

*Project supported by the National Natural Science Foundation of China (Grant Nos. 60676058 and 61076090).
†Corresponding author. E-mail: bcli@ioe.ac.cn
© 2013 Chinese Physical Society and IOP Publishing Ltd

(PCR signals) were recorded as a function of the modulation frequency in the range between 1 Hz and 100 kHz.

As the excitation power was square-wave modulated in the experiment, theoretically, under the linear physical mechanism,[6] the detected PCR signal could be described as the sum of the odd-order terms of a cosine expansion

$$S_{\mathrm{PCR}}(t) = \sum_{i=1}^{\infty} (-1)^{(i-1)} A_{2i-1} \cos[2\pi(2i-1)f \cdot t + \Phi_{2i-1}], \quad (1)$$

where f is the modulation frequency, A_{2i-1} and Φ_{2i-1} are the amplitude and phase of the PCR signal detected and demodulated at frequency $(2i-1)f$, $(i = 1, 2, 3, \ldots)$. Experimentally, at frequency f, a total of 16 odd-order terms (from the first term to the thirty-first term) were recorded and re-combined to form the time-domain PCR waveform described by Eq. (1). Since only the AC part of the PCR signal was detected by LIA, the DC part was neglected. It is worth mentioning that experimentally the time-domain PCR waveform could not be directly recorded due to the low amplitude of the PCR signal.

3. Results and discussion

Experimentally, for the comparison of PCR signals under the same photon flux into samples, the reflectance R of all samples at 830 nm was measured with a high-precision spectrophotometer (Lambda 1050, Perkin Elmer), as shown in Fig. 1(a), and the PCR amplitudes were normalized by the value $(1-R)$. Due to the damage recovery and re-crystallization induced by thermal annealing, the reflectance values of implanted and annealed silicon wafers in each group were close to each other. The reflectance values for samples in Groups S1 and S2 which were thermally oxidized were approximately 26.0%, while that of samples in Group S3 that were not thermally oxidized was approximately 30.2%. Figure 1(b) shows the implantation dose dependence of the PCR amplitude normalized with $(1-R)$ at the lowest frequency for the samples in the three groups. In general, the PCR amplitude increases with increasing implantation dose. However, there is an abrupt amplitude enhancement at implantation dose 1×10^{14} cm^{-2} for each group. To better understand the implantation dose dependence of the PCR amplitude, the frequency dependencies of the PCR amplitude and phase, as well as the quasi-time-domain PCR waveform for each sample were measured and the results for Group S1 and Group S3 are presented in Figs. 2 and 3, respectively. The results for Group S2 are similar to those for Group S1 and are not presented. Due to the fact that only sixteen odd-order terms were used to obtain the quasi-time-domain PCR waveform, unrealistic high-frequency oscillations appear in the waveforms, as shown in Figs. 2(c) and 3(c). Still, the wavy quasi-time-domain waveforms can be fitted to an exponential function to extract an effective lifetime for each sample. It is worth mentioning that the response function of the experimental setup is measured by employing a diode laser operated at 1310-nm wavelength and its influences on the frequency dependencies of the PCR signals and on the time-domain waveforms are eliminated.[12] The values of the extracted effective lifetime for all samples are given in Fig. 4.

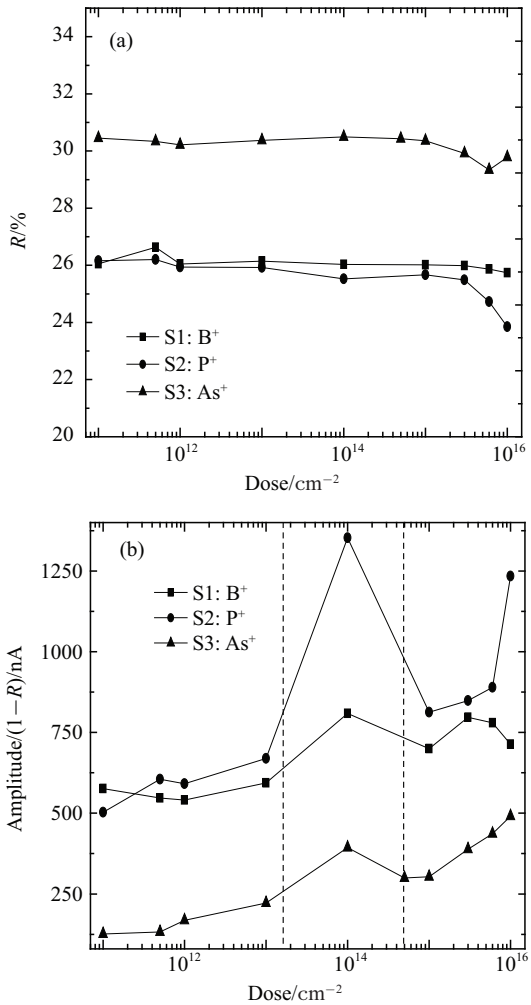


Fig. 1. Dependencies of (a) reflectance R and (b) PCR amplitude, normalized by value $(1-R)$, of all implanted and annealed samples in Groups S1, S2, and S3 on ion implantation dose.

In general, crystalline silicon ion implantation altered the optical and electrical properties at the surface, and in the sub-surface region,[13] as well as in the substrate[14] after thermal annealing. At 830 nm, the absorption coefficients of crystalline and amorphous silicon are approximately 7.6×10^4 m^{-1}[15] and 2.0×10^6 m^{-1},[15] respectively. Correspondingly, the penetration depth is approximately in the range from 500 nm to 13.2 μm, much deeper than the average depth of the implanted ions (below 100 nm, calculated by TRIM[16]) under implantation energy of 100 keV. However, due to transient enhanced diffusion (TED) mechanisms,[17,18] in thermally annealed silicon wafers implanted ions could spread deep into the substrates, and the depth of the diffused

ions might become close to the penetration depth of the excitation beam. The PCR signals of ion-implanted and thermally annealed silicon samples are mainly attributed to the substrate regions modified by the diffused ions. They are also affected by the implanted layer and the surface region via a carrier recombination mechanism.

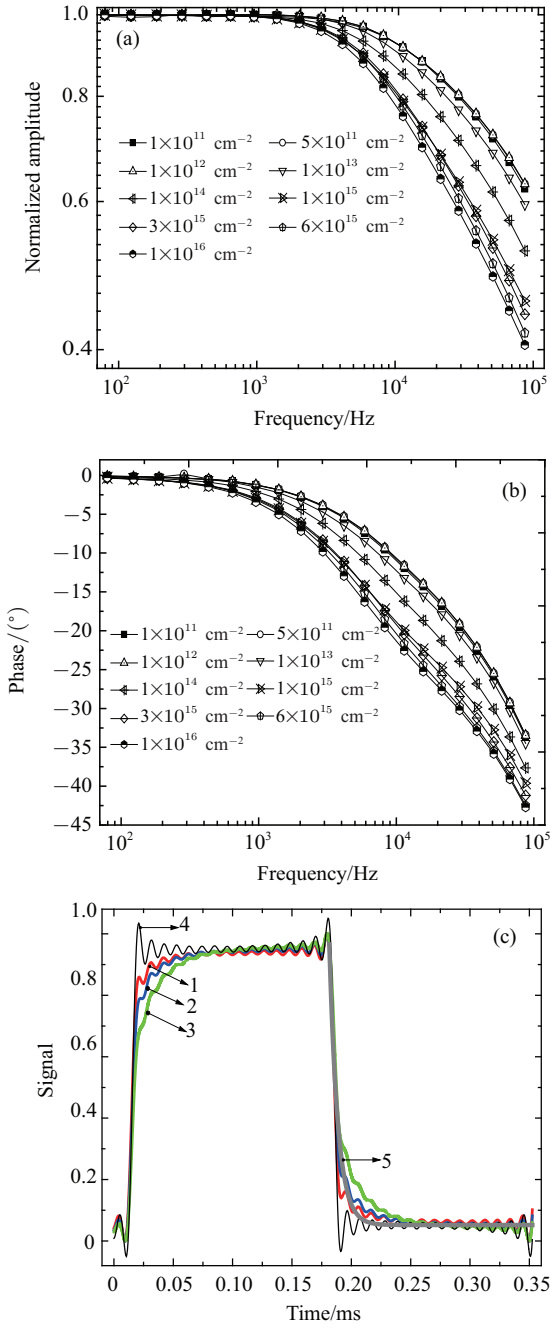


Fig. 2. (color online) Frequency dependencies of (a) normalized PCR amplitude and (b) phase for all samples in Group S1. (c) Normalized time-domain PCR waveforms for samples with ion implantation doses for B^+: 1×10^{11} cm^{-2} (curve 1), B^+: 1×10^{14} cm^{-2} (curve 2), B^+: 1×10^{16} cm^{-2} (curve 3), the response function of system (curve 4), and the best-fitted case (1×10^{11} cm^{-2}) (curve 5).

As figure 2 shows, at the low frequency end, both the normalized amplitude and phase of the PCR signal for B^+ implanted and thermally annealed silicon wafers are approximately independent of the modulation frequency. And the amplitude decreases and the phase lag increases with increasing frequency. As the implantation dose increases, the characteristic frequency where the PCR amplitude starts to decrease (and the PCR phase lag starts to increase) decreases. Meanwhile, the rising and falling rates of the normalized quasi-time-domain PCR waveform decrease. Similar results for P^+ implanted samples are also obtained but are not shown here. The evaluated effective lifetime

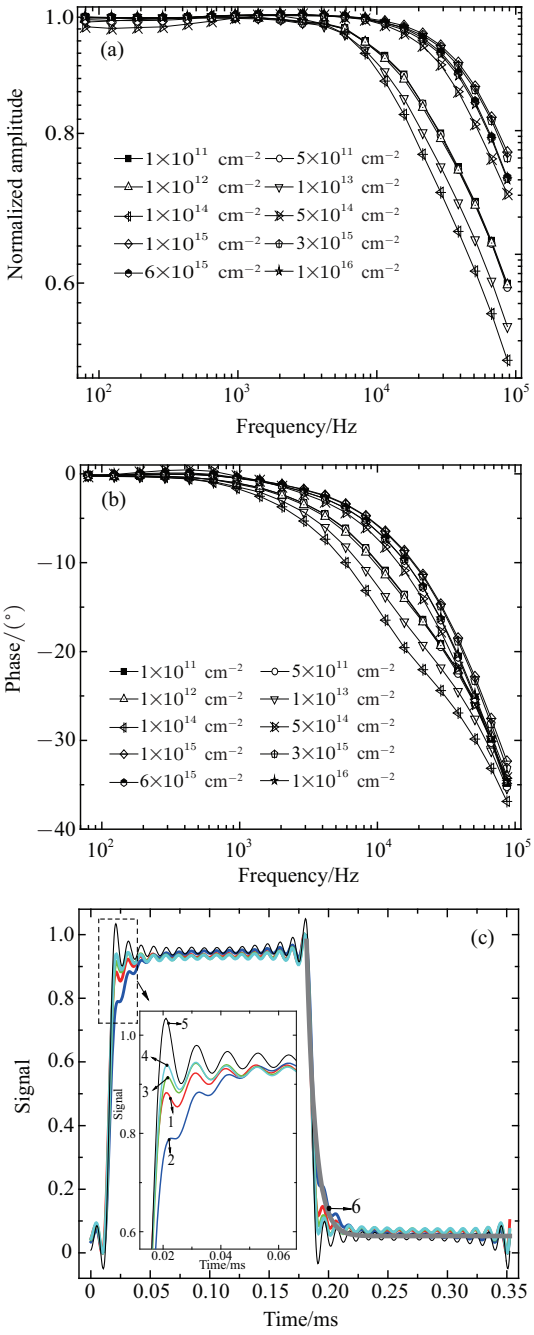


Fig. 3. (color online) Frequency dependencies of (a) normalized PCR amplitude and (b) phase for all samples in Group S3; (c) The normalized time-domain PCR waveforms for samples with ion implantation doses for As^+: 1×10^{11} cm^{-2} (curve 1), As^+: 1×10^{14} cm^{-2} (curve 2), As^+: 5×10^{14} cm^{-2} (curve 3), As^+: 1×10^{16} cm^{-2} (curve 4), the response function of system (curve 5), and the best-fitted case (1×10^{14} cm^{-2}) (curve 6).

increases monotonously from 5.2 μs to 10.5 μs for B^+ implanted samples and from 5.3 μs to 10.2 μs for P^+ implanted samples as presented in Fig. 4. Due to thermal annealing, the diffused B^+, P^+ ions alter the structural properties in the substrate region, and the effective lifetime related to those structural properties changes gradually with the increased dose. Of particular note, the PCR amplitude is abruptly enhanced at the dose 1×10^{14} cm^{-2}, where the effective lifetime significantly increases too. The implantation dose above the critical value about 2×10^{14} cm^{-2}[19] is a threshold for defects to appear, and the accumulation of defects leads to the formation of an amorphous layer. During thermal annealing at 1000 °C, {113} rodlike defects, faulted Frank dislocation loops and perfect dislocation loops located around the projected ion range[20] are formed due to recrystallization. The abrupt enhancement of PCR amplitude at dose 1×10^{14} cm^{-2} can be explained by the formation of many {113} rodlike defects[21] or dislocation loops , which provide spatial confinement of carriers[1] through a local strain field to enhance the photoluminescence, that is, the PCR signal. The damage saturates beyond the implantation dose 1×10^{14} cm^{-2}. A higher dose does not greatly change the effective lifetime or electronic properties. Simultaneously the number of dislocation loops, which enhance the photoluminescence, is reduced as the implantation dose further increases, and the PCR intensity slightly decreases with an implantation dose above 1×10^{14} cm^{-2}. Particularly, the PCR amplitude of the sample with P^+ implanted at dose 1×10^{16} cm^{-2} increases again, and the effective lifetime also increases as shown in Fig. 4. Those results may imply that another defect category exists at dose 1×10^{16} cm^{-2} that is different from the defect category at dose 1×10^{14} cm^{-2}, playing a dominant role in enhancing the photoluminescence.

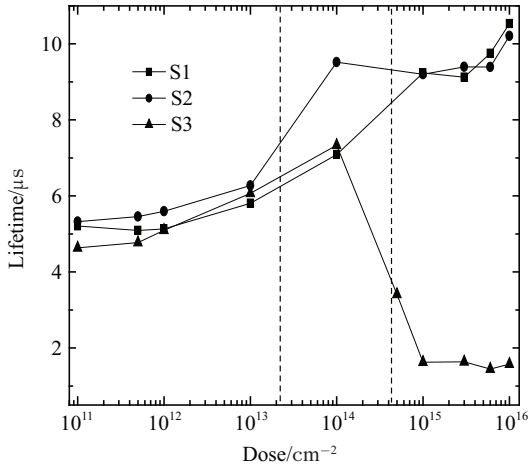


Fig. 4. Effective lifetime for all samples in groups S1, S2, and S3 extracted from the normalized time-domain PCR waveform profiles.

The effective lifetime behavior of As^+ implanted samples is significantly different from that of B^+ and P^+ implanted samples. When the implantation dose is above 1×10^{14} cm^{-2}, the effective lifetime decreases abruptly from 7.3 μs for dose 1×10^{14} cm^{-2} to 3.4 μs for dose 5×10^{14} cm^{-2}, and then stays at approximately 1.6 μs for doses 1×10^{15} cm^{-2} to 1×10^{16} cm^{-2}. As we know, compared with B^+, P^+ ions, the As^+ ion is heavier, with an atomic radius that is also larger than that of silicon. The amorphous layer appears with an implantation dose above 1×10^{14} cm^{-2},[22] in which case not all of the As^+ ions implanted into the substrate are fully activated by thermal annealing, resulting in a sharp decrease of the effective lifetime of the carriers. At the same time, experimentally, when As^+ implanted samples with doses above 5×10^{14} cm^{-2} are irradiated with the excitation beam, the PCR amplitudes increase rapidly with the irradiation time until they saturate after 4 to 10 minutes. In contrast, for B^+ and P^+ implanted samples, the PCR amplitudes are approximately independent of the irradiation time. Figure 5 shows the PCR amplitude versus irradiation time for As^+ implanted samples with doses from 1×10^{14} cm^{-2} to 1×10^{16} cm^{-2}, recorded at 2-kHz modulation frequency. For comparison, the results for B^+ and P^+ implanted samples with a dose of 1×10^{16} cm^{-2} are also presented. For this reason, the experimental data presented in Fig. 3 were recorded after the PCR signal stabilized. For As^+ implanted samples, the laser annealing effect is due to the intrinsic dangling-bond and lattice-disordered sub-surface states[23] created by As^+ implantation. A simple rate-equation model[24] with two types of traps generated from defects can be used to describe the fractional free carrier density at any time (t) as

$$\frac{n_{\mathrm{f}}(t)}{n_0} = 1 - \left[\frac{n_{01}}{n_0}\mathrm{e}^{-t/\tau_1} + \frac{n_{02}}{n_0}\mathrm{e}^{-t/\tau_2}\right], \qquad (2)$$

where n_{01} and n_{02} are the total number density of initial traps of type 1 and type 2, respectively, and n_0 represents the total

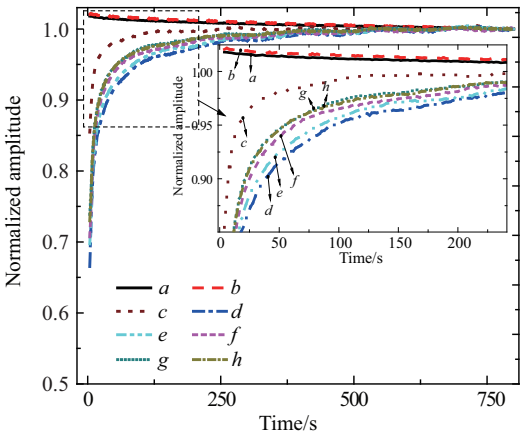


Fig. 5. (color online) Transient signals of PCR amplitude normalized to the last data point at frequency 2 kHz for B^+ and P^+ implanted samples with dose 1×10^{16} cm^{-2} and As^+ implanted samples with doses from 1×10^{14} cm^{-2} to 1×10^{16} cm^{-2} for P^+: 1×10^{16} cm^{-2} (curve *a*), B^+: 1×10^{16} cm^{-2} (curve *b*), As^+: 1×10^{14} cm^{-2} (curve *c*), As^+: 5×10^{14} cm^{-2} (curve *d*), As^+: 1×10^{15} cm^{-2} (curve *e*), As^+: 3×10^{15} cm^{-2} (curve *f*), As^+: 6×10^{15} cm^{-2} (curve *g*), and As^+: 1×10^{16} cm^{-2} (curve *h*).

number of trapped states as a constant, $n_f(t)$ is the instantaneous number density of excess free carriers liberated from the annealed traps, τ_1 and τ_2 are the lifetimes of the traps of types 1 and 2, respectively.

The experimental transient data (normalized) of As^+ implanted samples with doses 1×10^{14} cm^{-2} to 1×10^{16} cm^{-2} are fitted to Eq. (2), and the results are presented in Table 1. Apparently, the total fractional density $(n_{01}+n_{02})$ of traps and the trap lifetime (τ_1 and τ_2) of the samples with implantation doses from 5×10^{14} cm^{-2} to 1×10^{16} cm^{-2} are higher than those of the sample with dose 1×10^{14} cm^{-2}, resulting in shorter effective lifetimes, as presented in Fig. 4. It is clear that these results are associated with residual damage resulting from high-dose As^+ implantation and subsequent thermal annealing.

Table 1. The fitted trap lifetime and fractional density of the transient PCR signal for As^+ implanted samples with doses from 1×10^{14} cm^{-2} to 1×10^{16} cm^{-2}.

Implantation dose As^+/cm^{-2}	τ_1	τ_2	n_{01}	n_{02}	$n_{02}+n_{01}$
1×10^{14}	56.2	5.7	0.047	0.127	0.174
5×10^{14}	143.8	11.1	0.106	0.239	0.345
1×10^{15}	135.0	11.0	0.096	0.228	0.324
3×10^{15}	148.5	11.1	0.073	0.241	0.314
6×10^{15}	114.2	10.5	0.073	0.213	0.286
1×10^{16}	122.8	10.5	0.072	0.223	0.295

4. Conclusion

In summary, we have presented a combined frequency-swept and quasi-time-domain PCR technique and applied it to characterize thermally annealed silicon wafers with B^+, P^+, and As^+ ion implantation at doses ranging from 1×10^{11} cm^{-2} to 1×10^{16} cm^{-2}. The dependence of the effective lifetime on the implantation dose has been well explained by implantation induced defects and dislocation loops, and real-time monitoring of the transient PCR signals of the As^+ implanted samples with doses from 1×10^{14} cm^{-2} to 1×10^{16} cm^{-2} has also been carried out to relate the effective lifetime of the carriers to the trap density and lifetime. These comprehensive methods are useful for ion implantation monitoring in the fabrication of semiconductor devices, as well as helpful for the design and fabrication of silicon-based room-temperature light-emitting devices.

References

[1] Ng W L, Lourenço M A, Gwilliam R M, Ledain S, Shao G and Homewood K P 2001 *Nature* **410** 192

[2] Lourenço M A, Siddiqui M S A, Shao G, Gwilliam R M and Homewood K P 2004 *Phys. Stat. Sol. (a)* **201** 239

[3] Wang C, Yang Y, Yang R D, Li L, Xiong F and Bao J M 2011 *Chin. Phys. B* **20** 026802

[4] Lourenço M A, Milosavljević M, Shao G, Gwilliam R M and Homewood K P 2006 *Thin Solid Films* **504** 36

[5] Kveder V, Badylevich M, Steinman E, Izotov A, Seibt M and Schröter W 2004 *Appl. Phys. Lett.* **84** 2106

[6] Mandelis A, Batista J and Shaughnessy D 2003 *Phys. Rev. B* **67** 205208

[7] Li B C, Shaughnessy D, Mandelis A, Batista J and Garcia J 2004 *J. Appl. Phys.* **96** 186

[8] Liu X M, Li B C and Huang Q P 2010 *Chin. Phys. B* **19** 097201

[9] Huang Q P and Li B C 2011 *J. Appl. Phys.* **109** 023708

[10] Huang Q P and Li B C 2012 *J. Appl. Phys.* **111** 093729

[11] Shaughnessy D, Li B C, Mandelis A and Batista J 2004 *Appl. Phys. Lett.* **84** 5219

[12] Huang Q P and Li B C 2011 *Rev. Sci. Instrum.* **82** 043104

[13] Nastasi M and Mayer J W 2006 *Ion Implantation and Synthesis of Materials* (Berlin: Springer-Verlag)

[14] Stowe D, Fraser K, Galloway S, Senkader S, Falster R and Wilshaw P 2006 *Microscopy of Semiconducting Materials*: *Proceedings of the* 14*th Conference*, April 11–14, 2005, Oxford, UK, p. 335

[15] Palik E D 1998 *Handbook of Optical Constants of Solids* Vols. I and III (San Diego: Academic)

[16] Ziegler J F, Biersack J P and Littmark U 1985 *The Stopping Range of Ions in Solids* (Tarrytown: Pergamon); Ziegler J F 2006 http://www.srim.org

[17] Jain S C, Schenmaker W, Lindsay R, Stak P A, Decoutere S, Willander M and Maes H E 2002 *J. Appl. Phys.* **91** 8919

[18] Shao L, Liu J, Chen Q Y and Chu W K 2003 *Mater. Sci. Eng. R* **42** 65

[19] Jones K S, Prussin S and Weber E R 1988 *Appl. Phys. A: Solids Surf.* **45** 1

[20] Milosavljević M, Lourenco M A, Gwilliam R M and Homewood K P 2005 *J. Appl. Phys.* **97** 073512

[21] Pan G Z, Ostroumov R P, Lian Y G, Tu K N and Wang K L 2004 *Electron Devices Meeting*, December 13–15, 2004, Yokohama, Japan, pp. 343–346

[22] Pelaz L, Marqués L A and Barbolla J 2004 *J. Appl. Phys.* **96** 5947

[23] Opsal J, Taylor M W, Smith W L and Rosencwaig A 1987 *J. Appl. Phys.* **61** 240

[24] Rodriguez M E, Garcia J A, Mandelis A, Jean C and Riopel Y 1999 *Appl. Phys. Lett.* **74** 2429